Korean J. Chem. Eng., **26**(4), 946-954 (2009)
DOI: 10.1007/s11814-009-0158-y

A numerical study of the Dufour and Soret effects on unsteady natural convection flow past an isothermal vertical cylinder

Hari Ponnamma Rani*, and Chang Nyung Kim*,***,†**

*College of Advanced Technology, Kyung Hee University, Yongin 449-701, Korea
**Department of Mathematics and Humanities, National Institute of Technology, Waragal, India
***Industrial Liaison Research Institute, Kyung Hee University, Yongin 449-701, Korea
(*Received 15 October 2008 • accepted 31 December 2008*)

Abstract−The Dufour and Soret effects on the unsteady laminar free convective flow with mass transfer flow past a semi-infinite isothermal vertical cylinder were studied numerically. The governing partial differential equations were converted into a non-dimensional form and solved numerically by applying a Crank-Nicolson type of implicit finite-difference method with a tri-diagonal matrix manipulation and an iterative procedure. For the hydrogen-air mixture, which is a non-chemical reacting fluid, the profiles of the unsteady dimensionless velocity, temperature and concentration are shown graphically for the different values of thermal and mass Grashof numbers, thermal diffusion parameters (Soret numbers) and diffusion-thermo parameters (Dufour numbers). Finally, the simulated values of the average skin-friction coefficient, the average Nusselt number and the average Sherwood number are presented. The numerical results reveal that for an increasing Soret number or decreasing Dufour number, the time to reach the temporal maximum and the steady-state decreases for the flow variables. As the Soret number increases or the Dufour number decreases, both the skin friction and the Sherwood number increase, whereas the Nusselt number decreases.

Key words: Dufour Effect, Soret Effect, Transient, Natural Convection, Vertical Cylinder

INTRODUCTION

Combined heat and mass transfer in natural convection flow over a vertical cylinder is an important problem due to its important engineering applications, such as chemical and drying processes. Several steady state analyses for the flow over the vertical cylinder can be found in the literature. Bottemanne [1] studied the combined heat and mass transfer in the steady laminar boundary layer of a vertical cylinder placed in still air. The natural convection flows adjacent to the vertical surface, which result from the combined buoyancy effects of thermal and mass diffusion, were investigated by Gebhart and Pera [2]. Chen and Yuh [3] considered the steady heat and mass transfer processes near a vertical cylinder with uniform wall heat and mass fluxes. Their numerical solutions covered a wide range of radii and Prandtl numbers. While the steady-state analysis for the flow over a cylinder has been studied in detail, the transient analysis has also been paid attention to. Goldstein and Briggs [4] carried out the one-dimensional analytical study of transient natural convection from infinite cylinders. Dring and Gebhart [5] presented experimental results of the transient average temperature of Nichrome wires in silicone oils and in air. Subsequently, Velusamy and Garg [6] solved numerically the transient boundary layer equations for free convection flow past the heat generating vertical cylinder. The rate of propagation of the leading edge effect was given special consideration by them.

The previous studies, dealing with the transport phenomena of momentum and heat transfer, dealt with one component phases which possess a natural tendency to reach equilibrium conditions. However, there are activities, especially in industrial and chemical engineering processes, where a system contains two or more components whose concentrations vary from point to point. In such a system there is a natural tendency for the mass to be transferred and to minimize the concentration differences within the system. When heat and mass transfer occur simultaneously in a moving fluid, the relations between the fluxes and the driving potentials are of a more intricate nature. It has been found that an energy flux can be generated not only by temperature gradients but also by composition gradients. The energy flux caused by a composition gradient is called the Dufour or diffusion-thermo effect. On the other hand, mass flux can also be produced by temperature gradients and this is the Soret or thermal-diffusion effect. In general, the thermal-diffusion and the diffusion-thermo effects are of a smaller order of magnitude than the effects described by Fourier's law or Fick's law and are often neglected in the heat and mass-transfer processes. However, there are some exceptions. Anghel et al. [7], Dursunkaya and Worek [8], Eckert and Drake [9] and Postelnicu [10] have shown that the diffusion-thermo effect was recently found to be of a magnitude that cannot be neglected. The thermal-diffusion effect, for instance, has been utilized for isotope separation, and in mixture between gases with very light molecular weight (H_2, He) and of medium molecular weight (N_2, air).

Seddeek [11] has investigated the problem of thermal-diffusion and diffusion-thermo effects on the mixed free-forced convection and mass transfer in the presence of suction and blowing. Also, Eldabe et al. [12] have studied these effects for non-Newtonian fluid with the temperature dependent viscosity. Alam et al. [13] have studied the Dufour and Soret effects on steady MHD free convective heat and mass transfer flow past a semi-infinite vertical porous plate embedded in a porous medium. Salem [14] has also considered the

†To whom correspondence should be addressed.
E-mail: cnkim@khu.ac.kr

thermal-diffusion and diffusion-thermo effects on the convective heat and mass transfer in a viscoelastic fluid flow through a porous medium over a stretching sheet.

From the previous studies it can be noticed that generally less attention was paid to the problem of unsteady natural convection along a vertical cylinder under the combined heat and mass transfer flow with Soret and Dufour effects. Hence, the objective of the present work is to investigate the thermal-diffusion and diffusion-thermo effects on the unsteady laminar free convective and mass transfer boundary-layer flow along the vertical semi-infinite isothermal cylinder. In the present analysis, consideration is given to the situation in which the surface of the cylinder is maintained at a uniform temperature and concentration.

In Section 2 the mathematical formulation of the problem is presented. Also, the equations of mass, momentum, energy and species concentration for the incompressible fluid flow past a semi-infinite vertical cylinder are detailed in this section. The governing equations are first transformed into a non-dimensional form and then they are solved by an implicit finite-difference method, which is detailed in section 3. To support the current numerical calculations, corroborative evidence is provided in the results and discussion section, section 4. Numerical calculations are carried out for a hydrogen-air mixture, which has been selected as non-chemically reacting fluid pair. Emphasis has been placed on the influence of the dimensionless parameters such as Du (Dufour number), So (Soret number), Gr (thermal Grashof number) and Gc (mass Grashof number) on the flow field variables and heat and mass transfer coefficients. Finally, the concluding remarks are made. The analysis of the results revealed that the flow field is appreciably influenced by the abovementioned parameters.

FORMULATION OF THE PROBLEM AND GOVERNING EQUATIONS

An unsteady two-dimensional laminar combined heat and mass transfer boundary layer flow of a viscous incompressible fluid past an isothermal semi-infinite vertical cylinder of radius r_0 is considered as shown in Fig. 1. The x-axis is measured vertically upward along the axis of the cylinder. The origin of x is taken to be at the leading edge of the cylinder, where the boundary layer thickness is zero. The radial coordinate r is measured perpendicular to the axis of the cylinder. Initially, at time $t'=0$, it is assumed that the cylinder and the fluid are at the same surrounding ambient temperature T'_∞ and concentration C'_∞. When $t'>0$, the temperature and concentration of the cylinder are maintained to be at T'_w ($>T'_\infty$) and C'_w ($>C'_\infty$), respectively. It is assumed that the effect of viscous dissipation is negligible in the energy equation. The concentration C' of the diffusing species is assumed very small in the binary mixture and there is no chemical reaction between the diffusing species and the fluid. With the Boussinesq approximation and the above assumptions, the transient natural convection boundary layer equations are written as

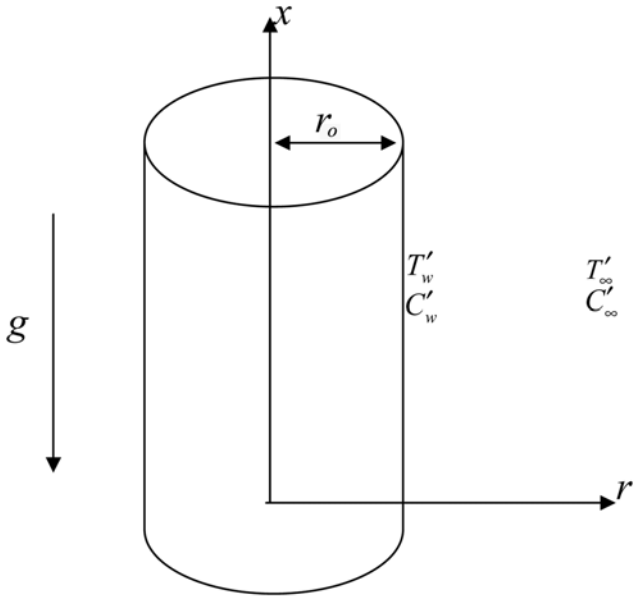

Fig. 1. Schematic of the investigated problem.

$$\frac{\partial(ru)}{\partial x}+\frac{\partial(rv)}{\partial r}=0 \tag{1}$$

$$\frac{\partial u}{\partial t'}+u\frac{\partial u}{\partial x}+v\frac{\partial u}{\partial r}=g\beta(T'-T'_\infty)+g\beta^*(C'-C'_\infty)+\frac{\upsilon}{r}\frac{\partial}{\partial r}\left(r\frac{\partial u}{\partial r}\right) \tag{2}$$

$$\frac{\partial T'}{\partial t'}+u\frac{\partial T'}{\partial x}+v\frac{\partial T'}{\partial r}=\frac{\alpha}{r}\frac{\partial}{\partial r}\left(r\frac{\partial T'}{\partial r}\right)+\frac{D_m k_T}{c_s c_p}\frac{1}{r}\frac{\partial}{\partial r}\left(r\frac{\partial C'}{\partial r}\right) \tag{3}$$

$$\frac{\partial C'}{\partial t'}+u\frac{\partial C'}{\partial x}+v\frac{\partial C'}{\partial r}=\frac{D_m}{r}\frac{\partial}{\partial r}\left(r\frac{\partial C'}{\partial r}\right)+\frac{D_m k_T}{T'_m}\frac{1}{r}\frac{\partial}{\partial r}\left(r\frac{\partial T'}{\partial r}\right) \tag{4}$$

where u and v are the velocity components parallel to x and r coordinates, respectively, g the acceleration due to gravity, β is the volumetric coefficient of thermal expansion, β^* is coefficient of expansion with concentration, υ is the reference kinematic viscosity, α the thermal diffusivity, D_m the coefficient of mass diffusivity, T'_m the mean fluid temperature, k_T the thermal diffusion ratio (i.e., thermal to mass concentration diffusion coefficients), c_p the specific heat at constant pressure and c_s the concentration susceptibility.

The last term on the right-hand side of the energy Eq. (3) and the diffusion Eq. (4) signifies the Dufour or diffusion-thermo effect and the Soret or thermal-diffusion effect, respectively.

The initial and boundary conditions are given by

$$\begin{aligned}
&t'\le 0:\ u=0,\ v=0,\ T'=T'_\infty,\ C'=C'_\infty \text{ for all x and r}\\
&t'>0:\ u=0,\ v=0,\ T'=T'_w,\ C'=C'_w \text{ at } r=r_0\\
&\qquad u=0,\ v=0,\ T'=T'_\infty,\ C'=C'_\infty \text{ at } x=0\\
&\qquad u\to 0,\ v\to 0,\ T'\to T'_\infty,\ C'\to C'_\infty \text{ as } r\to\infty
\end{aligned} \tag{5}$$

The non-dimensional variables are defined as

$$X=\frac{x}{r_0},\ R=\frac{r}{r_0},\ U=\frac{ur_0}{\upsilon},\ V=\frac{vr_0}{\upsilon},\ t=\frac{\upsilon t'}{r_0^2},\ T=\frac{T'-T'_\infty}{T'_w-T'_\infty},$$
$$C=\frac{C'-C'_\infty}{C'_w-C'_\infty} \tag{6}$$

and the non-dimensional parameters are defined as

$$Gr=\frac{g\beta r_0^3(T'_w-T'_\infty)}{\upsilon^2}\ \text{(thermal Grashof number)}$$

$$Gc=\frac{g\beta^* r_0^3(C'_w-C'_\infty)}{\upsilon^2}\ \text{(mass Grashof number)}$$

$$\mathrm{Pr}=\frac{\upsilon}{\alpha}\ \text{(Prandtl number)}$$

$$\mathrm{Sc}=\frac{\upsilon}{\mathrm{D}_m}\ \text{(Schmidt number)}$$

$$\mathrm{So}=\frac{\mathrm{D}_m\mathrm{k}_T(\mathrm{T}'_w-\mathrm{T}'_\infty)}{\upsilon\mathrm{T}'_m(\mathrm{C}'_w-\mathrm{C}'_\infty)}\ \text{(Soret number)}$$

$$\mathrm{Du}=\frac{\mathrm{D}_m\mathrm{k}_T(\mathrm{C}'_w-\mathrm{C}'_\infty)}{\upsilon\mathrm{c}_s\mathrm{c}_p(\mathrm{T}'_w-\mathrm{T}'_\infty)}\ \text{(Dufour number)} \tag{7}$$

By introducing the above non-dimensional Eqs. (6) and (7) into the Eqs. (1)-(4), they are reduced to the following form.

$$\frac{\partial(\mathrm{RU})}{\partial\mathrm{X}}+\frac{\partial(\mathrm{RV})}{\partial\mathrm{R}}=0 \tag{8}$$

$$\frac{\partial\mathrm{U}}{\partial\mathrm{t}}+\mathrm{U}\frac{\partial\mathrm{U}}{\partial\mathrm{X}}+\mathrm{V}\frac{\partial\mathrm{U}}{\partial\mathrm{R}}=\mathrm{GrT}+\mathrm{GcC}+\left(\frac{\partial^2\mathrm{U}}{\partial\mathrm{R}^2}+\frac{1}{\mathrm{R}}\frac{\partial\mathrm{U}}{\partial\mathrm{R}}\right) \tag{9}$$

$$\frac{\partial\mathrm{T}}{\partial\mathrm{t}}+\mathrm{U}\frac{\partial\mathrm{T}}{\partial\mathrm{X}}+\mathrm{V}\frac{\partial\mathrm{T}}{\partial\mathrm{R}}=\frac{1}{\mathrm{Pr}}\left(\frac{\partial^2\mathrm{T}}{\partial\mathrm{R}^2}+\frac{1}{\mathrm{R}}\frac{\partial\mathrm{T}}{\partial\mathrm{R}}\right)+\mathrm{Du}\left(\frac{\partial^2\mathrm{C}}{\partial\mathrm{R}^2}+\frac{1}{\mathrm{R}}\frac{\partial\mathrm{C}}{\partial\mathrm{R}}\right) \tag{10}$$

$$\frac{\partial\mathrm{C}}{\partial\mathrm{t}}+\mathrm{U}\frac{\partial\mathrm{C}}{\partial\mathrm{X}}+\mathrm{V}\frac{\partial\mathrm{C}}{\partial\mathrm{R}}=\frac{1}{\mathrm{Sc}}\left(\frac{\partial^2\mathrm{C}}{\partial\mathrm{R}^2}+\frac{1}{\mathrm{R}}\frac{\partial\mathrm{C}}{\partial\mathrm{R}}\right)+\mathrm{So}\left(\frac{\partial^2\mathrm{T}}{\partial\mathrm{R}^2}+\frac{1}{\mathrm{R}}\frac{\partial\mathrm{T}}{\partial\mathrm{R}}\right) \tag{11}$$

The corresponding initial and boundary conditions in the non-dimensional quantities are given by

$$\begin{aligned}&\mathrm{t}\le 0\text{: U=0, V=0, T=0, C=0 for all X and R}\\&\mathrm{t}>0\text{: U=0, V=0, T=1, C=1 at R=1}\\&\qquad\text{U=0, V=0, T=0, C=0 at X=0}\\&\qquad\mathrm{U}\to 0,\ \mathrm{V}\to 0,\ \mathrm{T}\to 0,\ \mathrm{C}\to 0\text{ as }\mathrm{R}\to\infty\end{aligned} \tag{12}$$

NUMERICAL SOLUTION OF THE PROBLEM

To solve the unsteady coupled non-linear governing Eqs. (8)-(11) an implicit finite difference scheme of Crank-Nicolson type has been employed. The finite difference equations corresponding to Eqs. (8)-(11) are as follows:

$$\frac{\mathrm{U}^{k+1}_{i,j}-\mathrm{U}^{k+1}_{i-1,j}+\mathrm{U}^{k}_{i,j}-\mathrm{U}^{k}_{i-1,j}}{2\Delta\mathrm{X}}+\frac{\mathrm{V}^{k+1}_{i,j}-\mathrm{V}^{k+1}_{i,j-1}+\mathrm{V}^{k}_{i,j}-\mathrm{V}^{k}_{i,j-1}}{2\Delta\mathrm{X}}+\frac{\mathrm{V}^{k+1}_{i,j}+\mathrm{V}^{k}_{i,j}}{2[1+(\mathrm{j}-1)\Delta\mathrm{R}]}=0 \tag{13}$$

$$\begin{aligned}&\frac{\mathrm{U}^{k+1}_{i,j}-\mathrm{U}^{k}_{i,j}}{\Delta\mathrm{t}}+\frac{\mathrm{U}^{k}_{i,j}}{2\Delta\mathrm{X}}(\mathrm{U}^{k+1}_{i,j}-\mathrm{U}^{k+1}_{i-1,j}+\mathrm{U}^{k}_{i,j}-\mathrm{U}^{k}_{i-1,j})\\&\quad+\frac{\mathrm{V}^{k}_{i,j}}{4\Delta\mathrm{R}}(\mathrm{U}^{k+1}_{i,j+1}-\mathrm{U}^{k+1}_{i,j-1}+\mathrm{U}^{k}_{i,j+1}-\mathrm{U}^{k}_{i,j-1})\\&\quad=\mathrm{Gr}\frac{\mathrm{T}^{k+1}_{i,j}+\mathrm{T}^{k}_{i,j}}{2}+\mathrm{Gc}\frac{\mathrm{C}^{k+1}_{i,j}+\mathrm{C}^{k}_{i,j}}{2}\\&\quad+\frac{\mathrm{U}^{k+1}_{i,j-1}-2\mathrm{U}^{k+1}_{i,j}+\mathrm{U}^{k+1}_{i,j+1}+\mathrm{U}^{k}_{i,j-1}-2\mathrm{U}^{k}_{i,j}+\mathrm{U}^{k}_{i,j+1}}{2(\Delta\mathrm{R})^2}\\&\quad+\frac{\mathrm{U}^{k+1}_{i,j+1}-\mathrm{U}^{k+1}_{i,j-1}+\mathrm{U}^{k}_{i,j+1}-\mathrm{U}^{k}_{i,j-1}}{4[1+(\mathrm{j}-1)\Delta\mathrm{R}]\Delta\mathrm{R}}\end{aligned} \tag{14}$$

$$\begin{aligned}&\frac{\mathrm{T}^{k+1}_{i,j}-\mathrm{T}^{k}_{i,j}}{\Delta\mathrm{t}}+\frac{\mathrm{U}^{k}_{i,j}}{2\Delta\mathrm{X}}(\mathrm{T}^{k+1}_{i,j}-\mathrm{T}^{k+1}_{i-1,j}+\mathrm{T}^{k}_{i,j}-\mathrm{T}^{k}_{i-1,j})\\&\quad+\frac{\mathrm{V}^{k}_{i,j}}{4\Delta\mathrm{R}}(\mathrm{T}^{k+1}_{i,j+1}-\mathrm{T}^{k+1}_{i,j-1}+\mathrm{T}^{k}_{i,j+1}-\mathrm{T}^{k}_{i,j-1})\\&\quad=\frac{(\mathrm{T}^{k+1}_{i,j-1}-2\mathrm{T}^{k+1}_{i,j}+\mathrm{T}^{k+1}_{i,j+1}+\mathrm{T}^{k}_{i,j-1}-2\mathrm{T}^{k}_{i,j}+\mathrm{T}^{k}_{i,j+1})}{2\mathrm{Pr}(\Delta\mathrm{R})^2}\\&\quad+\frac{(\mathrm{T}^{k+1}_{i,j+1}-\mathrm{T}^{k+1}_{i,j-1}+\mathrm{T}^{k}_{i,j+1}-\mathrm{T}^{k}_{i,j-1})}{4\mathrm{Pr}[1+(\mathrm{j}-1)\Delta\mathrm{R}]\Delta\mathrm{R}}\\&\quad+\mathrm{Du}\frac{\mathrm{C}^{k+1}_{i,j-1}-2\mathrm{C}^{k+1}_{i,j}+\mathrm{C}^{k+1}_{i,j+1}+\mathrm{C}^{k}_{i,j-1}-2\mathrm{C}^{k}_{i,j}+\mathrm{C}^{k}_{i,j+1}}{2(\Delta\mathrm{R})^2}\\&\quad+\mathrm{Du}\frac{\mathrm{C}^{k+1}_{i,j+1}-\mathrm{C}^{k+1}_{i,j-1}+\mathrm{C}^{k+1}_{i,j+1}-\mathrm{C}^{k}_{i,j-1}}{4[1+(\mathrm{j}-1)\Delta\mathrm{R}]\Delta\mathrm{R}}\end{aligned} \tag{15}$$

$$\begin{aligned}&\frac{\mathrm{C}^{k+1}_{i,j}-\mathrm{C}^{k}_{i,j}}{\Delta\mathrm{t}}+\frac{\mathrm{U}^{k}_{i,j}}{2\Delta\mathrm{X}}(\mathrm{C}^{k+1}_{i,j}-\mathrm{C}^{k+1}_{i-1,j}+\mathrm{C}^{k}_{i,j}-\mathrm{C}^{k}_{i-1,j})\\&\quad+\frac{\mathrm{V}^{k}_{i,j}}{4\Delta\mathrm{R}}(\mathrm{C}^{k+1}_{i,j+1}-\mathrm{C}^{k+1}_{i,j-1}+\mathrm{C}^{k}_{i,j+1}-\mathrm{C}^{k}_{i,j-1})\\&\quad=\frac{(\mathrm{C}^{k+1}_{i,j-1}-2\mathrm{C}^{k+1}_{i,j}+\mathrm{C}^{k+1}_{i,j+1}+\mathrm{C}^{k}_{i,j-1}-2\mathrm{C}^{k}_{i,j}+\mathrm{C}^{k}_{i,j+1})}{2\mathrm{Sc}(\Delta\mathrm{R})^2}\\&\quad+\frac{(\mathrm{C}^{k+1}_{i,j+1}-\mathrm{C}^{k+1}_{i,j-1}+\mathrm{C}^{k}_{i,j+1}-\mathrm{C}^{k}_{i,j-1})}{4\mathrm{Sc}[1+(\mathrm{j}-1)\Delta\mathrm{R}]\Delta\mathrm{R}}\\&\quad+\mathrm{So}\frac{\mathrm{T}^{k+1}_{i,j-1}-2\mathrm{T}^{k+1}_{i,j}+\mathrm{T}^{k+1}_{i,j+1}+\mathrm{T}^{k}_{i,j-1}-2\mathrm{T}^{k}_{i,j}+\mathrm{T}^{k}_{i,j+1}}{2(\Delta\mathrm{R})^2}\\&\quad+\mathrm{So}\frac{\mathrm{T}^{k+1}_{i,j+1}-\mathrm{T}^{k+1}_{i,j-1}+\mathrm{T}^{k+1}_{i,j+1}-\mathrm{T}^{k}_{i,j-1}}{4[1+(\mathrm{j}-1)\Delta\mathrm{R}]\Delta\mathrm{R}}\end{aligned} \tag{16}$$

The region of integration for the present problem is considered as a rectangle composed of the lines indicating X_{min}=0, X_{max}=1, R_{min}= 1 and R_{max}=16. Note that the non-dimensional axial position X is expressed as in Eq. (5). Here X_{max}=1 is chosen arbitrarily. The R_{max}= 16 practically corresponds to R=∞, which lies far from the momentum and energy boundary layers. In the above Eqs. (13)-(16) the subscripts i and j designate the grid points along the X and R coordinates, respectively, where X=iΔX and R=1+(j−1)ΔR and the superscript k designates a value of the time t (=kΔt), with ΔX, ΔR and Δt denoting the mesh sizes in the X, R and t axes, respectively. To obtain an economical and reliable grid system for the computations, a grid independence test has been performed. The steady-state velocity and temperature values obtained with the grid system of 100×500 differ in the second decimal place from those with the grid system of 50×250, and differ in the fifth decimal place from those with the grid system of 200×1,000. Hence the grid system of 100×500 has been selected for all subsequent analyses, with ΔX= 0.01, ΔR=0.03. Also, the time step size dependency has been carried out, which yields Δt=0.01 for reliable result.

From the initial conditions given in Eq. (12), the values of velocity U, V, temperature T and concentration C are known at time t= 0, then the values of C, T, U and V at the next time step can be calculated. Generally, when the above flow variables are known at t= kΔt, the value of these variables at t=(k+1)Δt is calculated as follows. The finite difference Eqs. (14), (15) and (16) at every internal nodal point on a particular *i*-level constitute a tri-diagonal system of equations. Such a system of equations is solved by Thomas algorithm (Carnahan et al. [15]). At first, the concentration C is calculated from Eq. (16) at every j nodal point on a particular *i*-level at the (k+1)th time step. Then, the temperature T is calculated from Eq. (15) at every j nodal point on a particular *i*-level at the (k+1)th time step, by using the updated values of concentration. By making use of these known values of C and T, the velocity U at the (k+

1)th time step is calculated from Eq. (14) in a similar manner. Thus, the values of C, T and U are known at a particular *i*-level. Then the velocity V is calculated from Eq. (13) explicitly. This process is repeated for the consecutive *i*-levels. Thus, the values of C, T, U and V are known at all grid points in the rectangular region at the (k+1)th time step. This iterative procedure is repeated for the successive time steps until the steady-state solution is reached.

To avoid the divergence of the solutions, the under-relaxation method is employed during the iterative process for all the flow variables. At the (k+1)th time step the values of U, V and T are obtained from the following equation.

$$\left.\begin{aligned} U^{k+1(=new)} &= U^k + p_U(U^{k+1} - U^k) \\ V^{k+1(=new)} &= V^k + p_V(V^{k+1} - V^k) \\ T^{k+1(=new)} &= U^k + p_T(T^{k+1} - T^k) \end{aligned}\right\} \quad (16)$$

where p_U, p_V, and p_T denote the under-relaxation factors for U, V and T, respectively. The steady-state solution is assumed to have been reached when the absolute difference between the values of velocity as well as temperature at two consecutive time steps is less than 10^{-5} at all grid points.

The local truncation error is $O(\Delta t^2+\Delta R^2+\Delta X)$ and it tends to zero as Δt, ΔR and ΔX tend to zero, which shows that the system is compatible. Also, the Crank-Nicolson type of implicit finite difference scheme is proved to be unconditionally stable for a natural convective flow where there is always a non-negative value of axial velocity (U) and a non-positive value of radial velocity (V) (Ganesan and Rani [16]). Thus, the currently employed scheme ensures convergence. The computations for the current problem have been carried out on an Intel Pentium 4 CPU 3.20 GHz computer system for different values of the parameters for the Dufour and Soret effects.

RESULTS AND DISCUSSION

To get an insight into the physical situation of the problem, the numerical values of the velocity, temperature and concentration are calculated for the different values of dimensionless parameters. The dimensionless numbers Du (Dufour number) and So (Soret number), which represent the diffusion-thermo and thermal-diffusion effect, respectively, can take, by their definition, arbitrary values, provided that the value of their product is kept to be constant (Kafoussias and Williams [17]). So, for the problem under consideration their product is assumed to be constant (=0.6), provided that the mean temperature T'_m and the reference temperature T'_∞ are kept constant. The influences of the dimensionless parameters Gr, Gc, So and Du on the flow field are analyzed for Pr=0.71 (air) and for Sc=0.22. The value of the Schmidt number is chosen to represent hydrogen in the air at approx. 25 °C and 1 atm (Gebhart [18]). The dimensionless parameters Gr and Gc take the values 5, 10 and 15 in the present calculations.

The present numerical results are validated by comparing them with the available steady state results. In Figs. 2 and 3 the present temperature and concentration profiles and the local Nusselt (Nu) and Sherwood (Sh) numbers, respectively, are compared with those of Chen and Yuh [3] for Gr=Gc=10, Pr=0.7, Sc=0.2, So=0.0 and Du=0.0. The agreement between the previous results and the present numerical results is found to be good.

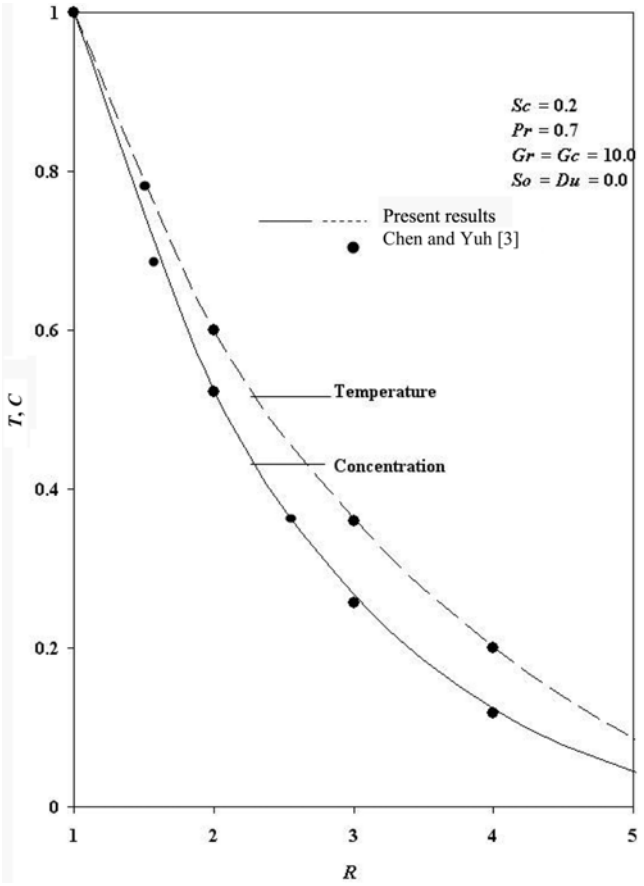

Fig. 2. Comparison of the temperature and concentration profiles.

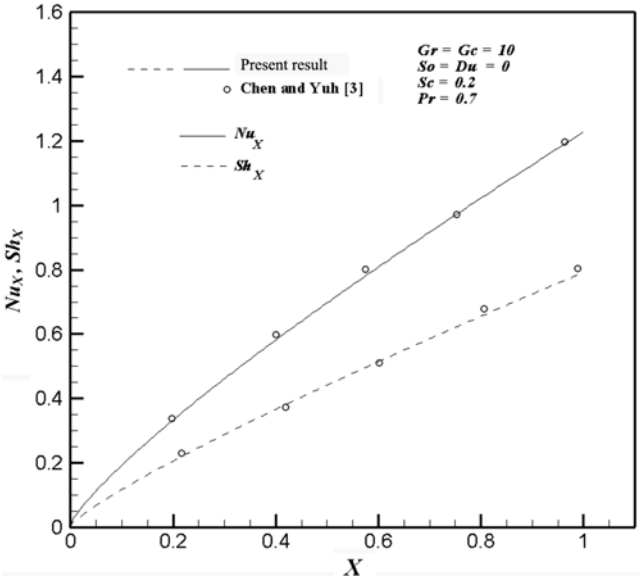

Fig. 3. Comparison of the Nusselt (Nu) and Sherwood number (Sh).

The simulated transient dimensionless velocity, temperature and concentration variations at the different locations for Gr=Gc=10, Du=0.15 and So=0.4 is presented in Figs. 4-6, respectively, against the dimensionless time. It is observed that at all the locations the

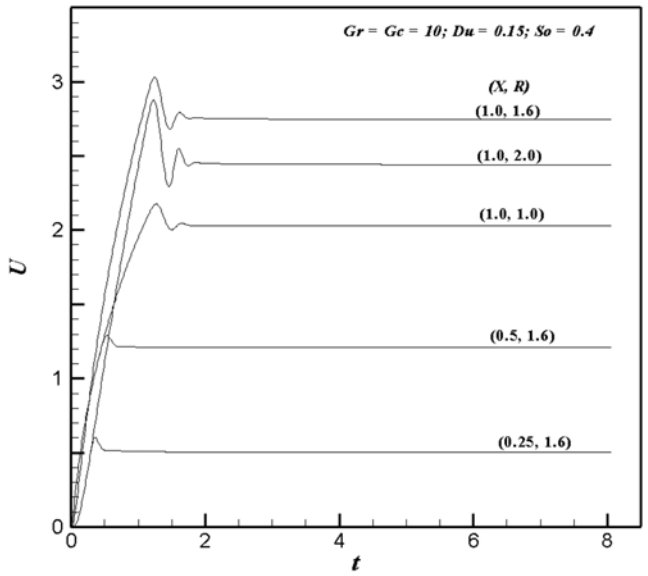

Fig. 4. The transient velocity at different locations with respect to time for fixed values of dimensionless parameters.

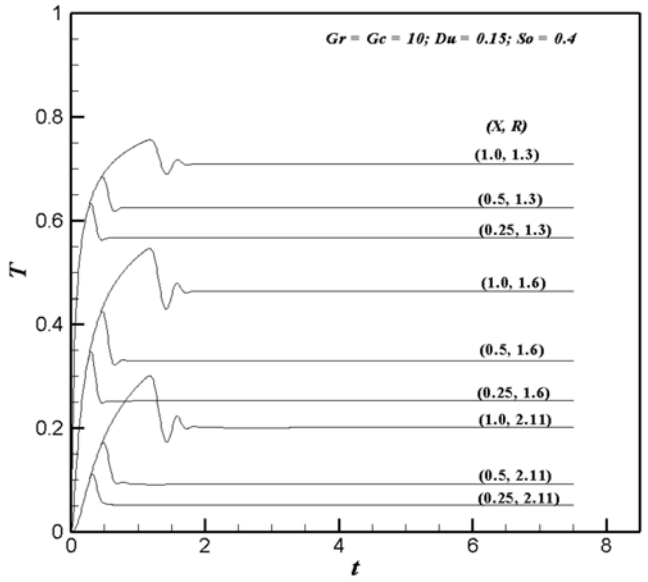

Fig. 5. The transient temperature at different locations with respect to time for fixed values of dimensionless parameters.

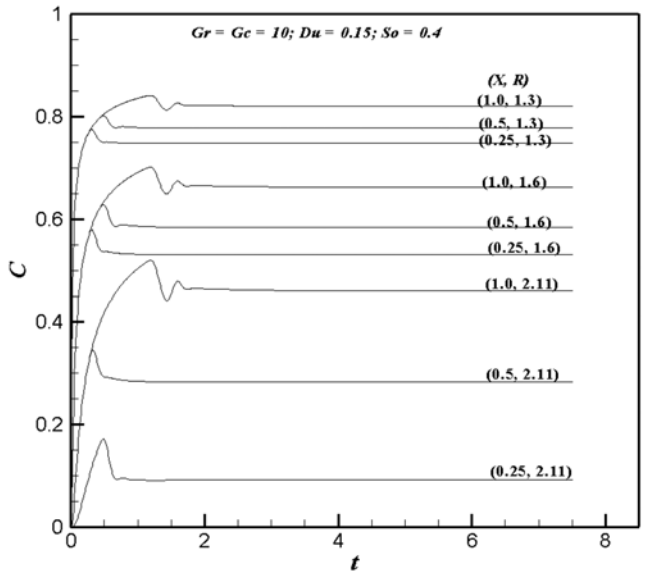

Fig. 6. The transient concentration at different locations with respect to time for fixed values of dimensionless parameters.

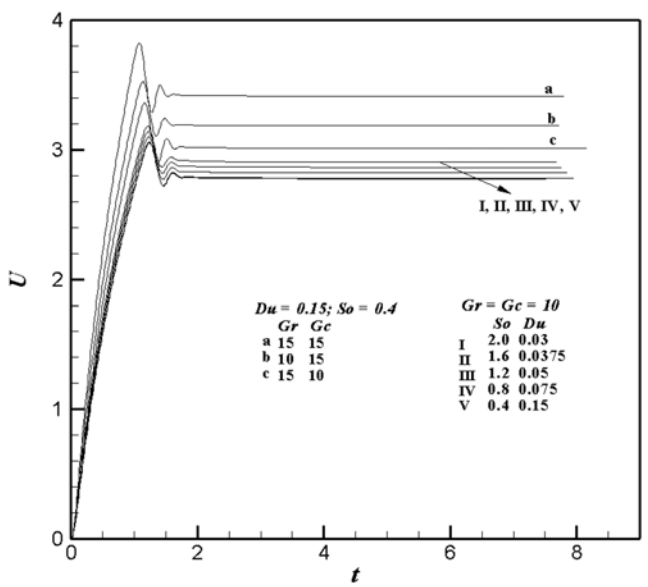

Fig. 7. The transient velocity for different dimensionless parameters with respect to time at (1.0, 1.6).

velocity, temperature and concentration increase with time, reach the temporal maximum, then decrease and after slight fluctuation reach the asymptotic steady-state. The velocity, temperature and concentration profiles increase with the increasing axial position. From Figs. 5 and 6 it can be observed that at the beginning there is no difference in the temperature and concentration profiles for the radial positions, respectively, with respect to the time. These results imply that at the beginning the conduction and diffusion are dominant in the flow field.

The simulated transient dimensionless velocity, temperature and concentration variation for different parameters are shown in Figs. 7-9, respectively, against the time. For all values of the dimensionless parameters the velocity increases with time, reaches the temporal maximum, then decreases and after slight fluctuation reaches the asymptotic steady-state. It can be noted that the temporal maximum and steady-state values of the velocity increase with increasing values of Gr and Gc. Since the energy and concentration equations are independent of Gr and Gc except for the Dufour number and Soret number, the temperature and concentration profiles are shown only for different Du and So combinations with fixed values of Gr=Gc=10. As seen from Figs. 7-9 the temporal maximum and the steady state values of velocity and concentration are increasing but those of temperature are decreasing with increasing So. But the opposite trend is observed for the increasing Du. It can be noticed that the influence of Du and So is considerably noticeable on the transient velocity and concentration in comparison with the tran-

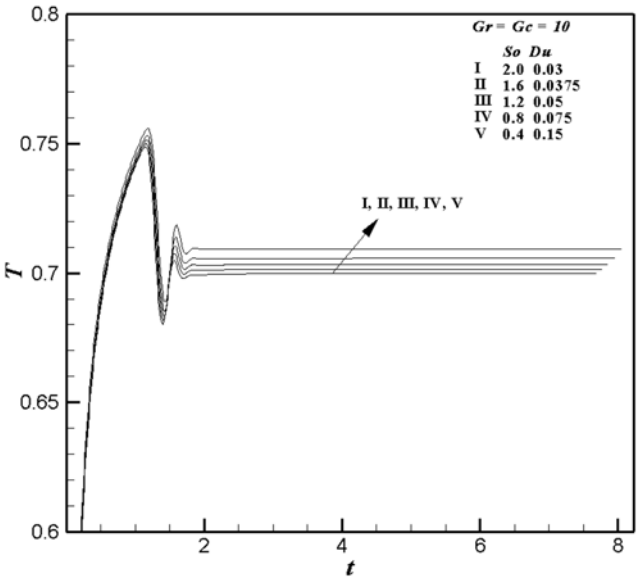

Fig. 8. The simulated transient temperature profiles for different dimensionless parameters with respect to time at (1.0, 1.3).

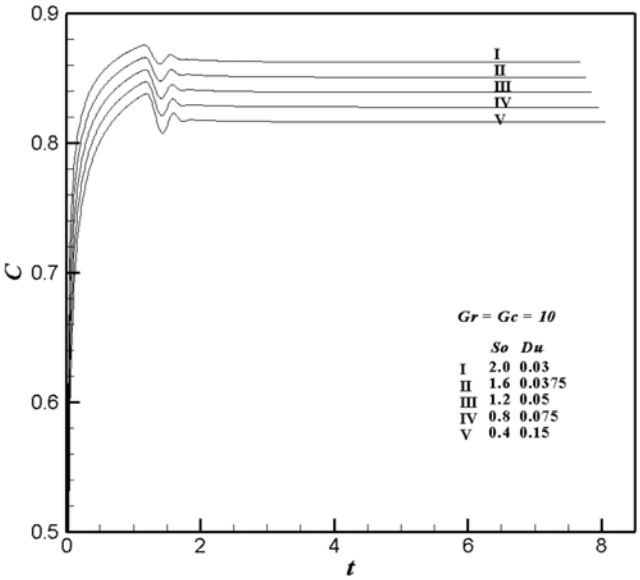

Fig. 9. The transient concentration profiles for different dimensionless parameters with respect to time at (1.0, 1.3).

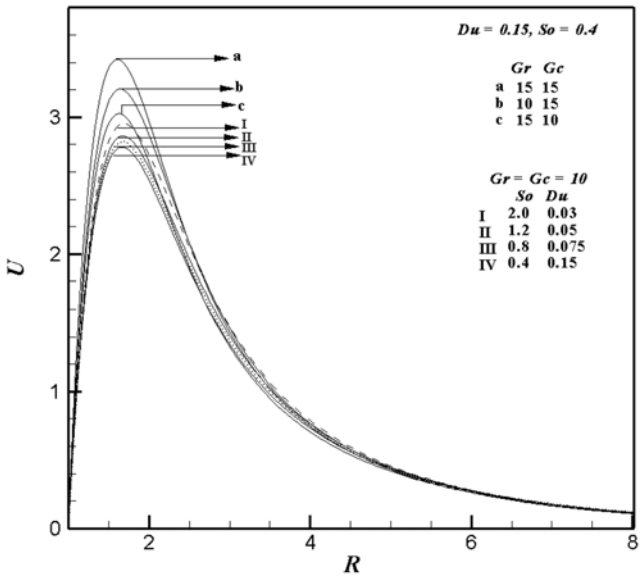

Fig. 10. The steady-state velocity profiles for different dimensionless parameters with respect to the radial coordinate at X= 1.0.

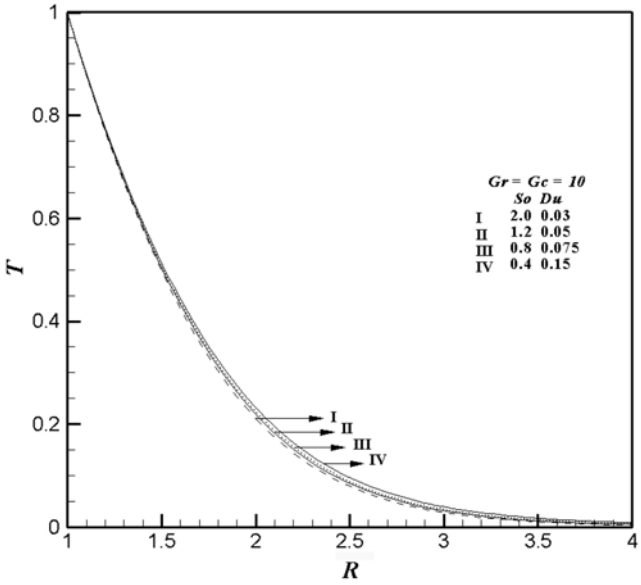

Fig. 11. The steady-state temperature profiles for different dimensionless parameters with respect to radial coordinate.

sient temperature.

Figs. 10-12 depict the steady-state velocity, temperature and concentration profiles against the radial coordinate for different parameters. With the increasing radial position the velocity increases and reaches the maximum value and then decreases monotonically. The temperature and the concentration profiles decrease with the radial position monotonically. It can be observed that the steady-state velocity increases as Gr and Gc increases. As shown, in these Figs. 10-12 the velocity and the concentration are increasing with the increasing So, but the temperature decreases as So increases. This behavior is a direct consequence of the Soret effect, which produces a mass flux from lower to higher solute concentration driven by the temperature gradient. Also, when So is high enough, the thermal and the solutal buoyancy forces combine their actions to enhance the convection velocity, which leads to the increase in the velocity of the fluid.

In Tables 1-3 the time for the flow variables U, T and C to reach the temporal maximum and the steady-state is tabulated with different Gr, Gc and So and Du combination, respectively. From Tables 1 and 2 it can be observed that with the increasing values of Gr and Gc the time for all the flow variables to reach the temporal maximum decreases, while the time to reach the steady state increases for increasing Gr and for decreasing Gc. From Table 3 it is observed that for the decreasing So or increasing Du, the time to reach the temporal maximum of the flow variables and the steady-state in-

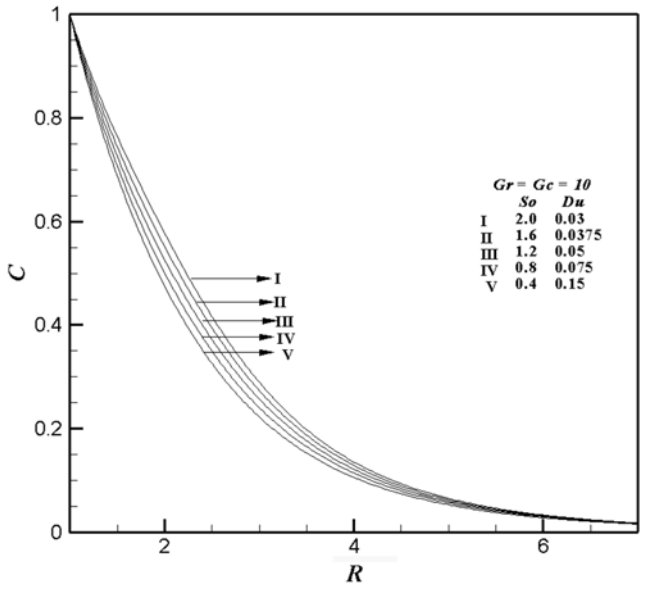

Fig. 12. The steady-state concentration profiles for different dimensionless parameters with respect to radial coordinate.

Table 1. Time (t) to reach the temporal maximum of velocity (U), temperature (T) and concentration (C) and the steady state for different values of Gr with Gc=10, So=0.15 and Du= 0.4

Gr	Temporal maximum (t) of			Steady state time (t)
	U	T	C	
5	1.36	1.29	1.30	7.94
10	1.25	1.18	1.20	8.06
15	1.18	1.11	1.12	8.16
20	1.10	1.04	1.06	8.23

Table 2. Time (t) to reach the temporal maximum of velocity (U), temperature (T) and concentration (C) and the steady state for different values of Gc with Gr=10, So=0.15 and Du= 0.4

Gc	Temporal maximum (t) of			Steady state time (t)
	U	T	C	
5	1.36	1.35	1.36	8.79
10	1.25	1.18	1.20	8.06
15	1.14	1.08	1.09	7.73
20	1.06	1.01	1.01	7.52

creases slightly.

For engineering purposes, one is usually more interested in the values of the skin-friction coefficient, heat transfer rate and mass transfer rate than in the velocity, temperature and concentration profiles. For the present problem these skin-friction coefficient, heat transfer rate and mass transfer rate are derived in the following equations.

The wall shear stress at the wall can be expressed as

$$\tau_w = \left(\mu \frac{\partial u}{\partial r}\right)_{r=r_0} \tag{17}$$

Table 3. Time (t) to reach the temporal maximum of velocity (U), temperature (T) and concentration (C) and the steady state for different So and Du combinations with Gc=Gr=10

So	Du	Temporal maximum (t) of			Steady state time (t)
		U	T	C	
2.00	0.03	1.24	1.15	1.16	7.69
1.60	0.0375	1.25	1.16	1.17	7.77
1.20	0.05	1.25	1.17	1.17	7.86
0.80	0.075	1.26	1.18	1.18	7.96
0.50	0.12	1.27	1.18	1.19	8.04
0.40	0.15	1.27	1.18	1.19	8.06
0.20	0.30	1.27	1.19	1.19	8.08

By introducing the non-dimensional quantities given in Eqs. (6) and (7) in the above Eq. (17), we get

$$\tau_w = \frac{\mu^2}{\rho r_0^2}\left(\frac{\partial U}{\partial R}\right)_{R=1} \tag{18}$$

Considering $\mu^2/\rho r_0^2$ to be the characteristic shear stress, then the skin-friction coefficient can be written as

$$C_f = \left(\frac{\partial U}{\partial R}\right)_{R=1} \tag{19}$$

The integration of the Eq. (19) from X=0 to X=1 gives the following average skin-friction coefficient.

$$\overline{C_f} = \int_0^1 \left(\frac{\partial U}{\partial R}\right)_{R=1} dX \tag{20}$$

The Nusselt number can be written as follows:

$$Nu_x = \frac{\dot{q}_w}{k_T(T'_w - T'_\infty)/r_0} \tag{21}$$

where the heat transfer $\dot{q}_w = -k_T\left(\frac{\partial T'}{\partial r}\right)_{r=r_0} = -k_T \frac{T'_w - T'_\infty}{r_0}\left(\frac{\partial T}{\partial R}\right)_{R=1}$

Thus, with the non-dimensional quantities introduced before, Eq. (21) can be written as

$$Nu_x = -\left(\frac{\partial T}{\partial R}\right)_{R=1} \tag{22}$$

The integration of the above Eq. (22) with respect to X yields the following average Nusselt number.

$$\overline{Nu} = -\int_0^1 \left(\frac{\partial T}{\partial R}\right)_{R=1} dX \tag{23}$$

The Sherwood number can be written as follows:

$$Sh_x = \frac{\dot{m}_w}{D_m(C'_w - C'_\infty)/r_0} \tag{24}$$

where the mass transfer $\dot{m}_w = -D_m\left(\frac{\partial C'}{\partial r}\right)_{r=r_0} = -D_m \frac{C'_w - C'_\infty}{r_0}\left(\frac{\partial C}{\partial R}\right)_{R=1}$

Thus, in the same way Eq. (24) can be written as

$$Sh_x = -\left(\frac{\partial C}{\partial R}\right)_{R=1} \tag{25}$$

The integration of the above Eq. (25) with respect to X yields the following average Sherwood number.

$$\overline{Sh} = -\int_0^1 \left(\frac{\partial C}{\partial R}\right)_{R=1} dX \tag{26}$$

The derivatives involved in the Eqs. (20), (23) and (26) are evaluated by using a five-point approximation formula and then the integrals are evaluated with the Newton-Cotes closed integration formula. The simulated non-dimensional average skin-friction coefficient ($\overline{C_f}$), the average heat transfer rate ($\overline{Nu}$) and the average mass transfer rate ($\overline{Sh}$) have been plotted against the time in Figs. 13-15, respectively, for different non-dimensional parameters. It is seen from these figures that either by increasing So or by decreasing Du, the value of average skin-friction coefficient is increasing, while the values of average Nusselt number and Sherwood number are decreasing. Further, increasing either of Gr or Gc causes $\overline{C_f}$ to increase, which is in line with the velocity profiles plotted in Fig. 10.

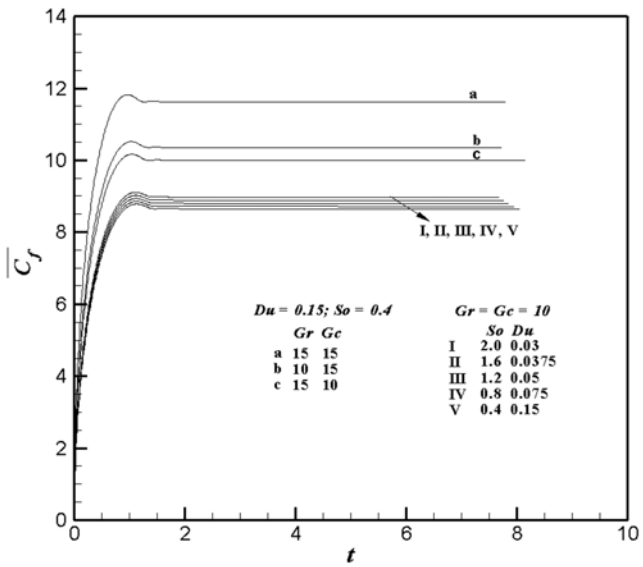

Fig. 13. The average skin-friction coefficient with respect to time.

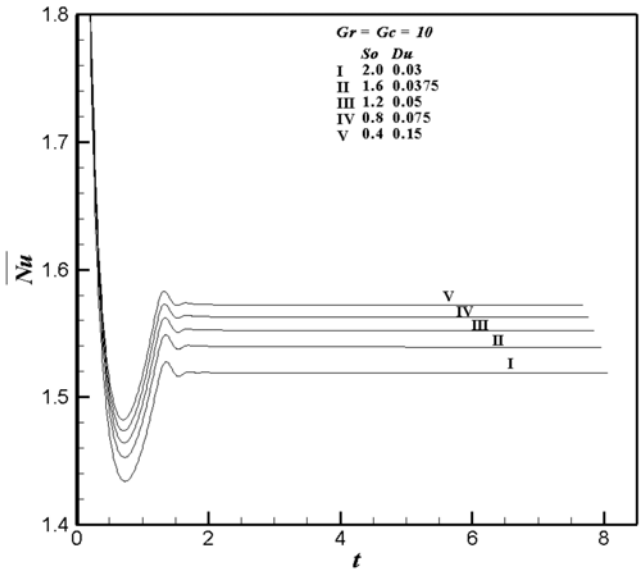

Fig. 14. The average Nusselt number with respect to time.

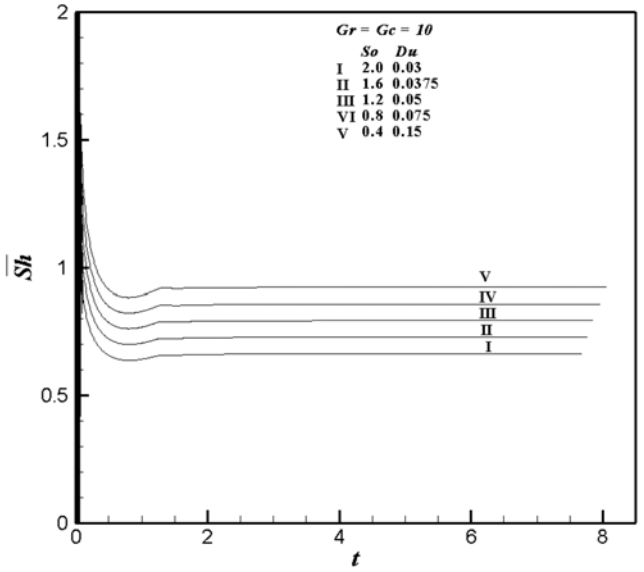

Fig. 15. The average Sherwood number with respect to time.

From Fig. 13 it can be seen that for all dimensionless parameters, $\overline{C_f}$ increases monotonically from zero, attains the temporal maximum and after slight fluctuation reaches the asymptotic steady-state value. Fig. 14 shows that the average Nusselt number, at the beginning, decreases drastically and increases again, after slight fluctuation reaches the steady state. Also, from Fig. 15 the $\overline{Sh}$ decreases monotonically, then after slight fluctuation, reaches the asymptotic steady state.

CONCLUSIONS

The problem of thermal-diffusion and diffusion-thermo effects on the convective heat and mass transfer in a hydrogen-air mixture fluid past the semi-infinite vertical cylinder has been investigated numerically. A Crank-Nicolson type of the implicit method is used to solve the dimensionless governing equations in a meridian plane. The effects of different parameters such as Soret number, Dufour number, thermal Grashof number (Gr) and mass Grashof number (Gc) on the velocity, temperature and concentration profiles are analyzed. The following points were noticed from the present simulated results.

With the increasing values of Gr or Gc, the time to reach the temporal maximum of all the flow variables decreases, while the time to reach the steady state increases for increasing Gr or decreasing Gc. An increase in the values of Gr or Gc results in an increase in the velocity profiles. For the increasing Soret number or the decreasing Dufour number, the time to reach the temporal maximum of the flow variables and the steady-state decreases. Also, with the increasing Soret number or the decreasing Dufour number, the velocity and the concentration profiles are increasing, but the temperature decreases. The influence of Soret number or the Dufour number is less on the temperature profiles in comparison with the velocity and concentration profiles. The concentration and Sherwood num-

ber are more affected by Soret number. As the Soret number increases or Dufour number decreases, both the skin friction and the Sherwood number increase, whereas the Nusselt number decreases.

From the present study, it is observed that the thermal-diffusion and diffusion-thermo effects have to be considered in the heat and mass transfer problems, otherwise they will introduce a substantial error. These secondary effects along with the thermal and mass Grashof numbers of a working fluid have turned out to be sensitive in a natural convection heat and mass transfer problem. Hence, these effects have to be taken into consideration in order to predict the skin friction coefficient, heat transfer rate and mass transfer rate accurately.

ACKNOWLEDGMENTS

This work was supported partially by the second stage BK21 program and partially by the Korea Science and Engineering Foundation (KOSEF) grant funded by the Korean Government (MEST) (No. R11-2008-098-00000-0).

REFERENCES

1. F. A. Bottemanne, *Appl. Sci. Res.*, **25**, 372 (1972).
2. B. Gebhart and L. Pera, *Int. J. Heat Mass Trans.*, **14**, 2025 (1971).
3. T. S. Chen and C. F. Yuh, *Int. J. Heat Mass Trans.*, **23**, 451 (1980).
4. R. J. Goldstein and D. G. Briggs, *J. Heat Trans.*, **86**, 490 (1964).
5. R. P. Dring and B. Gebhart, *Tran. ASME J. Heat Tran.*, **88**, 246 (1966).
6. K. Velusamy and V. K. Garg, *Int. J. Heat Trans.*, **35**, 1293 (1992).
7. M. Anghel, H. S. Takhar and I. Pop, *Studia Universitatis Babes-Bolyai, Mathematica*, **XLV**(4), 11 (2000).
8. Z. Dursunkaya and W. M. Worek, *Int. J. Heat Mass Trans.*, **35**, 2060 (1992).
9. E. R. G. Eckert and R. M. Drake, *Analysis of heat and mass transfer*, McGraw-Hill, New York (1972).
10. A. Postelnicu, *Int. J. Heat Mass Trans.*, **47**, 1467 (2004).
11. M. A. Seddeek, *Acta Mechanica*, **172**, 83 (2004).
12. N. T. Eldabe, A. G. El-Saka and A. Fouad, *Appl. Math. Comput.*, **152**, 867 (2004).
13. M. S. Alam and M. M. Rahman, *Nonlinear Analysis: Modelling and Control*, **11**, 3 (2006).
14. A. M. Salem, *Commun. Numer. Meth. Engng.*, **22**, 955 (2006).
15. B. Carnahan, H. A. Luther and J. O. Wilkes, *Applied numerical methods*, John Wiley & Sons, New York (1969).
16. P. Ganesan and H. P. Rani, *Heat Mass Transfer*, **33**, 449 (1998).
17. N. G. Kafoussias and E. W. Williams, *Int. J. Engng. Sci.*, **33**, 1369 (1995).
18. B. Gebhart, *Heat transfer*, 2nd ed., McGraw-Hill, New York (1971).